Eur. Phys. J. E **22**, 41–49 (2007)
DOI: 10.1140/epje/e2007-00011-4

THE EUROPEAN PHYSICAL JOURNAL E

Formation and mobility of droplets on composite layered substrates

A. Yochelis[1,a], E. Knobloch[1], and L.M. Pismen[2]

[1] Department of Physics, University of California, Berkeley, CA 94720-7300, USA
[2] Department of Chemical Engineering and Minerva Center for Nonlinear Physics of Complex Systems, Technion - Israel Institute of Technology, 32000 Haifa, Israel

Received 20 August 2006 / Received in final form 16 January 2007
Published online: 21 February 2007 –

Abstract. A mesoscale fluid film placed on a solid support may break up and form droplets. In addition, droplets may exhibit spontaneous translation by modifying the wetting properties of the substrate, resulting in asymmetry in the contact angles. We examine mechanisms for droplet formation and motion on uniform and terraced landscapes, i.e., composite substrates. The fluid film stability, droplet formation and velocity are studied theoretically in the isothermal case using a lubrication approach in one spatial dimension. The droplet properties are found to involve contributions from both the terraced layer thickness and molecular interactions via the disjoining potential.

PACS. 47.55.dr Interactions with surfaces – 68.08.Bc Wetting – 47.55.np Contact lines – 47.15.gm Thin film flows

1 Introduction

Properties of liquid droplets on substrates are of scientific and technological interest in a variety of contexts [1]. Some of the challenging questions pertain to the impact of molecular interactions and substrate properties on the formation and mobility of the droplets [2]. Although it is well known that interfacial energy [3,4] drives the evolution of thin liquid films, there is no fundamental understanding of the explicit physics that is involved. The main complications are associated with the fluid description in the vicinity of the droplet contact line, where molecular scale processes at the liquid-substrate interface may drive bulk behavior [5,6].

Molecular interactions can be incorporated into a continuum fluid description through the *disjoining potential* of the liquid film [7]. The latter accounts for the physical/chemical properties of the system [8,9] and serves as the driving force for droplets by modifying their contact angles [10]. The disjoining potential can be computed within a mesoscopic dynamic diffuse interface theory [11] that takes advantage of the separation between the thickness of the mesoscopic layer and the horizontal scale of the bulk motion to reduce the Stokes equation to an equation for the evolution of the film thickness. As a consequence, physical or chemical properties incorporated into the disjoining potential are responsible for the rich behavior exhibited by the system, ranging from film rupture to droplet propagation. For example, propagation of mesoscopic droplets on uniform horizontal substrates can be triggered by (i) external gradients such as temperature gradients [12,13] or substrate heterogeneity [14,15], and (ii) spontaneous development of asymmetry between the front and rear contact angles [16–24].

Recently, a new mechanism for spreading [25] and self-propelled droplet motion [26] was reported in experiments with long-chain alkanes (wax), this system differs from others by the simultaneous coexistence of a thin fluid precursor, a relatively large droplet and a terraced solid layer, all of the same chemical composition. In this paper we focus on this novel setup. After presenting the model equations (Sect. 2) we investigate theoretically and numerically the formation of droplets (Sect. 3) and their mobility (Sect. 4). Our results include the conditions under which stationary droplets are expected, as well as an analytical expression for the velocity of a droplet straddling a terrace as a function of the terrace height, van der Waals interactions and droplet size. Although our analysis is motivated by experiments on long-chain alkanes, the ultimate results are not limited to a particular set of experiments, and are applicable to any system dominated by van der Waals interactions and terraced topography, as discussed in Section 5.

[a] *Present address*: Department of Medicine (Cardiology), University of California, Los Angeles, CA 90095, USA;
e-mail: yochelis@ucla.edu

2 Lubrication model

We start with a fluid model of the subregion with coexisting (under similar thermodynamic conditions) liquid and solid phases, as shown in Figure 1. Under weakly nonwetting conditions the fluid film breaks into droplets that coexist with a thinner precursor layer [5]. Such a situation arises, for example, in experiments with long-chain alkanes (C_nH_{2n+2}) placed on top of a silicon substrate [25]. The system includes (i) a bulk fluid droplet, (ii) ordered (smectic A in case of alkanes) layers formed as a result of surface freezing, and (iii) a molecularly thin but uniform precursor layer.

To describe the formation of the droplet, we make use of the lubrication approximation [4]. The approximation is applicable to liquid films with a large aspect ratio (i.e., thin films) provided the interface is only gently curved, implying a contact angle that is not too large, $\theta \sim \mathcal{O}(1)$. As a consequence, the pressure or, more generally, a driving potential can be taken to be constant across the layer in the vertical direction. The governing equation for the droplet height $h(\mathbf{x}, t)$ follows from mass conservation,

$$\partial_t h = -\nabla \cdot \mathbf{j}, \tag{1}$$

where $\mathbf{j}$ is the mass flux

$$\mathbf{j} = \eta^{-1} k(h) \nabla \left(\sigma \nabla^2 h - \mathit{\Pi} \right), \tag{2}$$

η is the dynamic viscosity, $k(h)$ is the mobility coefficient, σ is the surface tension, and $\mathit{\Pi}$ is the disjoining potential per unit volume. Computation of $\mathit{\Pi}$ is the key component for understanding the possible sources of variation in the droplet contact angles that triggers mobility.

In the following we consider a one-dimensional version of equation (1), and study the effect of an additional frozen layer that coexists under similar thermodynamic conditions with the fluid, as discussed in Appendix A. Scaling respectively h, x, t, $\mathit{\Pi}$ with d, d, $d\eta/\sigma$, σ/d, where d is a hard-core molecular diameter and identifying surface tension σ as the typical energy of missing chemical bonds at the fluid-vapor interface per typical molecular scale, $\sigma \sim k_B T/d^2$, equation (1) takes the nondimensional form [23]

$$\partial_t h = -\partial_x \left[k(h) \partial_x \left(\partial_{xx} h - \mathit{\Pi} \right) \right], \tag{3}$$

where

$$\mathit{\Pi} = \begin{cases} -\dfrac{3\beta n_0^2}{8\pi} \left[\dfrac{\chi}{(h-H)^3} + \dfrac{\chi_\alpha}{h^3} \right] & \text{for} \quad h > H+1, \\ -\dfrac{3\beta n}{8\pi} \left[n_0 (\chi + 1) - n + \dfrac{n_0 \chi_\alpha}{(1+H)^3} \right] & \\ + \dfrac{3n}{2\pi} \left[\dfrac{1}{1-n} - \ln\left(\dfrac{1}{n} - 1 \right) - 2\beta n - \mu_0 \right] & \\ & \text{for} \quad h \le H+1, \end{cases} \tag{4}$$

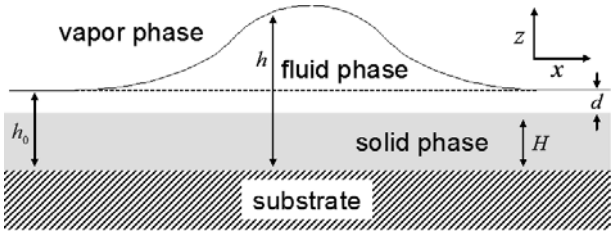

Fig. 1. A sketch of a droplet on top of a uniform solid layer of thickness H. The solid layer and fluid are assumed to consist of different phases of the same substance. The symbols h and $h_0 \equiv H + d$ denote the fluid bulk and precursor heights, where d is a molecular diameter.

and

$$k = \begin{cases} \lambda^2 (h - H) + \dfrac{1}{3} \left[h - (H+1) \right]^3 \text{ for } h > H+1, \\ \lambda^2 \text{ for } h \le H+1\,. \end{cases} \tag{5}$$

To obtain equations (4) and (5) we have introduced a dimensionless equilibrium chemical potential μ_0 at the liquid-vapor interface, together with the equilibrium fluid particle density n_0, inverse temperature β and the standard Hamaker constant χ, in addition to the effective Hamaker constant χ_α (for definitions, see Appendix A). In addition, we have also scaled the particle number density n by b^{-1}, and the dimensional quantities k and λ by d^3 and d, respectively [23]. In the following we assume that the nonwettability coefficient $|\chi|$ is small; this assumption implicitly defines the horizontal scale in the nondimensionalization. Thus the dimensionless disjoining potential $\mathit{\Pi}$ is in fact of order one. In the following we use the phenomenological prescription $n = n_0(h - H)$ to relate the density n in the precursor domain to the density above it, cf. [26].

3 Droplet formation on a uniform support

3.1 Wetting transitions

For a standard uniform substrate, with van der Waals interactions only, the sign of χ determines whether the substrate is wetting ($\chi > 0$) or nonwetting ($\chi < 0$); in both cases the transition is of second order [27–32], although the inclusion of additional interactions into the disjoining potential such as steric or polar forces may result in a first order transition [33]. For the present case the disjoining potential (4) corresponding to the nonwetting case is shown in Figure 2. Two different values of H and of the effective Hamaker constant χ_α are used. In all cases the effective thickness of the precursor layer h is close to $H+1$ (i.e., $H + d$ in real units), regardless of the sign of χ_α.

Although the potential is produced solely by van der Waals forces the composition of different layers within the support domain may change the nature of the wetting transition. For the weakly nonwetting case, $\chi < 0$, the choice of $\chi_\alpha < 0$ leads to a second order (smooth) phase

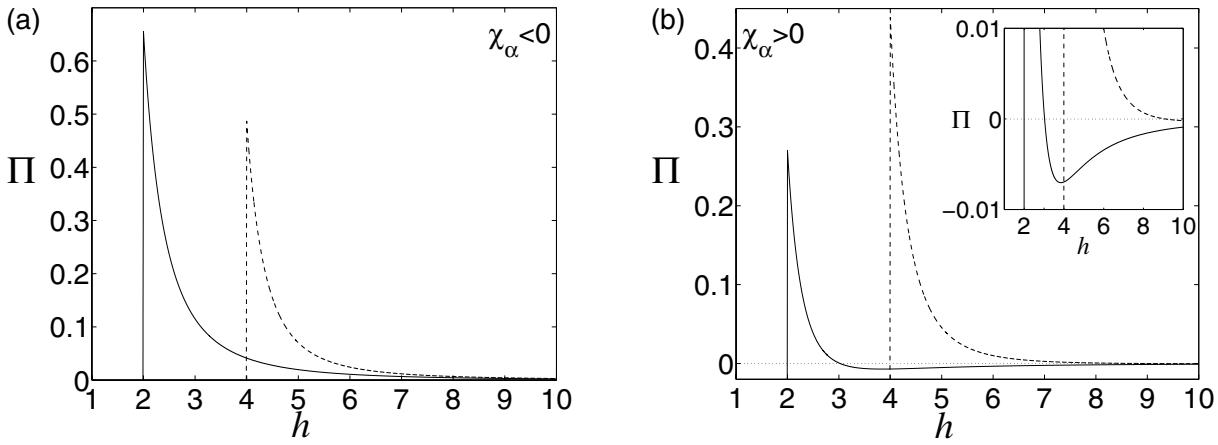

Fig. 2. The disjoining potential (4) for two values of the effective van der Waals interaction, χ_α, between the solid layer and the substrate. Two solid phase thicknesses are considered, $H = 1$ (solid line) and $H = 3$ (dashed line), so that the precursor thickness is given by $h_0 \simeq H + 1$. The inset in (b) shows a blow-up of the region in the vicinity of the equilibrium chemical potential $\mu = \mu_0$ or $\Pi = 0$. Parameters: $\beta = 15$, $\chi = -0.3$, $\mu_0 = -11.3636$, $n_0 = 0.9282$, $\lambda = \sqrt{3}$ and (a) $\chi_\alpha = -1$, (b) $\chi_\alpha = 1$.

transition (see Fig. 2a) while for $\chi_\alpha > 0$ we obtain a first order phase transition (see Fig. 2b). The main thin film implications are that in the former case the droplet resides on a thin precursor layer while in the latter case the droplet may coexist with a thicker film as well, due to bistability when $\Pi < 0$ (see inset in Fig. 2b). A similar situation also occurs in a liquid/vapor layered octane system [34].

3.2 Linear instability of a uniform film

While a thin precursor layer $h = h_0$ is stabilized by molecular forces, a thick liquid layer placed on a uniform substrate may exhibit rupture due to fluid-surface instability or the presence of impurities (defects) on the substrate surface [35–45]. Stability properties of a thick liquid layer of initial thickness $h = h_*$ may be determined by examining the evolution of infinitesimal perturbations of the form

$$h = h_* + \epsilon h_q e^{st+iqx} + c.c. + \mathcal{O}(\epsilon^2), \tag{6}$$

where s is the perturbation growth rate and $\epsilon \ll 1$. From equation (3) we obtain the dispersion relation

$$s(q) = -k(h_*)\, q^2 \left[\frac{\partial \Pi}{\partial h_*} + q^2\right]. \tag{7}$$

Since $k(h_*)$ is always positive a long wavelength instability develops when $\partial_{h_*}\Pi < 0$, i.e., when $\chi_\alpha < \chi^*_\alpha$, where

$$\chi^*_\alpha = -\frac{\chi h_*^4}{(h_* - H)^4}. \tag{8}$$

The instability threshold depends on the temperature via χ, on the substrate composition via H, as well as on the fluid height h_*, as shown in Figure 3.

As a solid layer begins to melt its thickness decreases, while the remaining solid surface becomes covered with a liquid layer, as shown in Figures 4a, 4b. Under appropriate

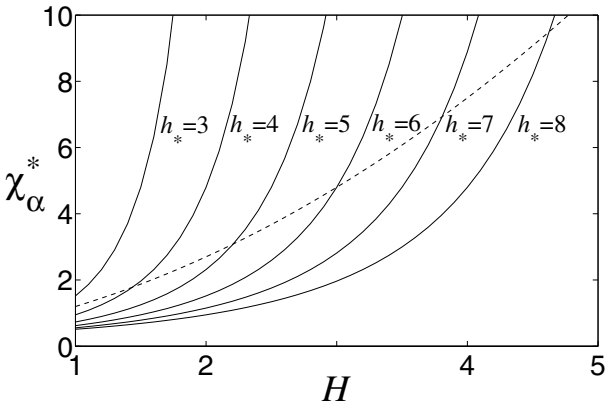

Fig. 3. The linear stability limit (8) as a function of the thickness H of the solid layer for $\chi = -0.3$ and several different values of the initial fluid height h_* (solid lines). The upper limit $(H+1)^2|\chi|$ (Eq. (10)) for the existence of steady droplets is shown as a dashed line.

conditions (see Eq. (8)) the resulting liquid layer breaks up into an array of droplets on top of a thin precursor layer, as shown by explicit numerical computation (see Appendix B) using equation (3) and illustrated in Figures 4c, 4d. The resulting droplets interact only weakly via the thin precursor, and any subsequent coarsening is extremely slow.

3.3 Contact angles and spreading

In the absence of other external forces, the droplet asymptotic contact angle for the weakly nonwetting case ($\chi < 0$, $|\chi| \ll 1$) reads [10,23]

$$\theta = \sqrt{2\int_{h_0}^{\infty} \Pi \; dh} = \sqrt{\frac{3\beta n_0^2|\chi|}{8\pi}}\sqrt{1 - \frac{\chi_\alpha/|\chi|}{(H+1)^2}}. \tag{9}$$

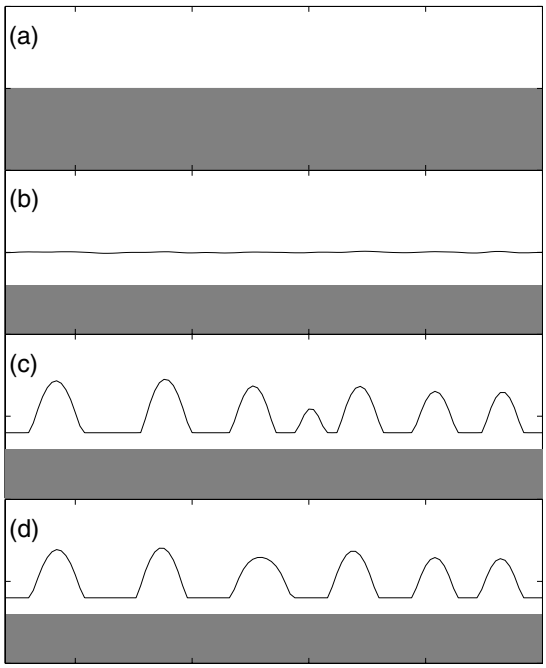

Fig. 4. (a) Thick solid layer (shaded region) on top of a substrate (not shown) that melts and leads to coexistence of a fluid film on top of a thin solid layer (b). (c, d) Numerical solution of equation (3) at $t = 500$, showing the linear instability of a weakly perturbed uniform fluid layer, $h_* = 5$, and the formation of droplets. The horizontal range is $x = [0, 230]$ and the vertical range is $h = [0, 10]$. Parameters: $\chi = -0.3$, $\beta = 15$, $\mu_0 = -11.3636$, $n_0 = 0.9282$, $\lambda = \sqrt{3}$, $H = 3$, (c) $\chi_\alpha = -1$ and (d) $\chi_\alpha = 1$.

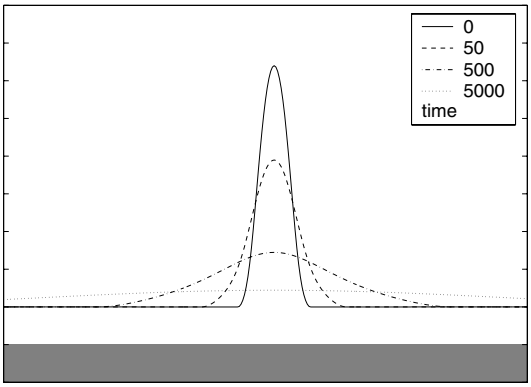

Fig. 5. Droplet spreading on top of a homogeneous support when $\chi_\alpha > (H+1)^2|\chi|$ and $\chi_\alpha > \chi_\alpha^*$, where χ_α^* is given by (8). The distinct lines correspond to numerical solutions of equation (3) at successive time intervals. The horizontal range is $x = [0, 300]$ and the vertical range is $h = [0, 10]$. Other parameters: $\chi = -0.3$, $\chi_\alpha = 5$, $\beta = 15$, $\mu_0 = -11.3636$, $n_0 = 0.9282$, $\lambda = \sqrt{3}$, and $H = 1$.

Thus when $\chi_\alpha < 0$ a solution for θ always exists, while for $\chi_\alpha > 0$ such solutions exist only for

$$0 < \chi_\alpha < (H+1)^2|\chi|. \tag{10}$$

In particular when $\chi_\alpha > (H+1)^2|\chi|$ no stationary droplets exist on a homogeneous support. Figure 5 shows, through numerical integration of equation (3), that in this case the droplet continuously spreads, as expected on the basis of Figure 3.

4 Droplet motion on a terraced landscape

In general, substrate homogeneity is an idealization, so that very often a heterogeneity in the form of a terraced landscape has to taken into account. A droplet placed on a terraced substrate will tend to move due to the difference in contact angles between the upper (H^+) and lower (H^-) terraces, or equivalently due to the asymmetry in the disjoining potential at the sides of the drop [23], see Figure 2. In particular, equation (9) shows that for fixed $\chi_\alpha < 0$ and $H^+ > H^-$ the contact angles satisfy $\theta(H^+) < \theta(H^-)$, and conversely for $\chi_\alpha > 0$. Thus the sign of χ_α (and hence the temperature) determines the sign of the contact angle asymmetry. The predictions of this asymmetry obtained from equation (9) on the assumption that the droplet profile is only weakly distorted, $\Delta H \equiv H^+ - H^- \ll a$, where a is the horizontal droplet radius (solid line in Fig. 6a), agree well with the mesoscopic contact angles computed from the slope at the inflection points of the drop profiles obtained numerically from equation (3) and shown in Figure 6b (points in Fig. 6a). These are computed with the upper terrace (H^+) on the left and the lower terrace (H^-) on the right.

The characteristic droplet velocity can be deduced from integral conditions based on the equilibrium solution [46]. This approach avoids the explicit solution of the dynamic equations and in particular the computation of the perturbed shape [47]. To derive an expression for the droplet velocity v, we look for solutions of the form $h = h(x - vt)$, where $|v| \ll 1$. Equation (3) can then be integrated yielding $vh = j$, assuming that no flux of liquid from infinity is present. This expression is a statement of local mass conservation in quasistationary motion. Equation (3) then yields the quasistationary equation

$$\frac{vh}{k(h)} = \partial_x \left[\partial_{xx} h - \Pi\right]. \tag{11}$$

In the following we use an integral relation obtained from this equation to compute the drop velocity v. To do so we break up the domain into three parts [48]: (i) droplet bulk; (ii) contact line region; and (iii) precursor region.

4.1 Thermodynamic driving forces

For a single droplet with a precursor film of thickness h_0, the integral relation defining the droplet mobility is obtained by multiplying equation (11) by $h - h_0$ and integrating over a large region centered on the droplet. While the first term on the right hand side of (11) vanishes [6] the second yields

$$-\int_{-\infty}^{\infty} (h - h_0) \frac{\partial \Pi}{\partial x} dx = \int_{h_0^+}^{h_0^-} (h_0 - h) \frac{\partial \Pi}{\partial h} dh = F^- - F^+, \tag{12}$$

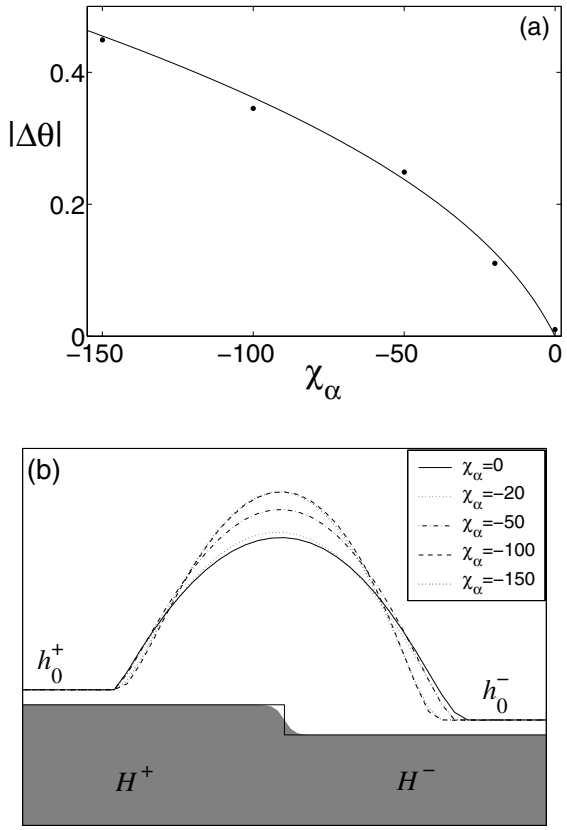

Fig. 6. (a) The contact angle difference $|\Delta\theta|$ on a terrace with $H^+ = 8$ and $H^- = 6$. The solid line represents the solution of equation (9) while the points show the slope at the inflection point calculated from the droplet profiles shown in (b), obtained by numerical integration of equation (3). In (b) the horizontal range is $x = [0, 80]$ and the vertical range is $h = [0, 25]$. Other parameters: $\beta = 15$, $\chi = -0.3$, $\mu_0 = -11.3636$, $n_0 = 0.9282$, and $\lambda = \sqrt{3}$.

where

$$F^{\pm} \equiv \int_{h_0^{\pm}}^{\infty} \left(h - h_0^{\pm}\right) \frac{\partial \Pi}{\partial h}\, dh = -\frac{1}{2}\left(\theta^{\pm}\right)^2 \qquad (13)$$

are the forces that arise in the vicinity of the droplet menisci on both sides of the terrace (see Fig. 6b). The lower integration limit is set by the uniform precursor thickness $h_0^{\pm}$ away from the drop ($x \to \mp\infty$). The error in extending the upper limit of integration in equation (13) to infinity is negligible due to the weak dependence of the disjoining potential at the center of a large liquid droplet on the film thickness.

4.2 Dissipation

In addition to the driving force computation in equation (13), we must also evaluate the dissipation integral

$$I = \int_{-\infty}^{\infty} \frac{h(h-h_0)}{k(h)} dx. \qquad (14)$$

Since the integrand vanishes in the precursor, the integral may be evaluated separately in the droplet bulk and the vicinity of the contact line, and matched at a point where the layer thickness lh_0 is much larger than the precursor thickness but much smaller than the maximum droplet height, i.e., $1 \ll l \ll a/h_0$. The location of the matching point must not affect the final result.

4.2.1 Contact line region

The contribution of the contact line (CL) region to the dissipation integral is given by

$$I_{CL}^{\pm} = \int_{h_0^{\pm}}^{lh_0^{\pm}} \frac{h(h-h_0^{\pm})}{k(h)\sqrt{y^{\pm}(h)}} dh, \qquad (15)$$

where $y = [h'(x)]^2$ represents a phase plane transformation variable [10] given to leading order by

$$\frac{dy^{\pm}}{dh} = 2\Pi^{\pm}(h), \qquad y(h_0^{\pm}) = 0. \qquad (16)$$

Near the contact lines we may further simplify the calculation by writing $h = \widetilde{h} + H^{\pm}$. The solution of equation (16) is then

$$y^{\pm} = \frac{3\beta n_0^2 |\chi|}{8\pi}\left[\frac{\widetilde{\chi}}{(\widetilde{h}+H^{\pm})^2} - \frac{1}{\widetilde{h}^2} + 1 - \frac{\widetilde{\chi}}{(1+H^{\pm})^2}\right], \qquad (17)$$

where $\widetilde{\chi} = \chi_\alpha/|\chi|$ and we have taken $h_0^{\pm} = H^{\pm} + 1$. The quantity (15) thus reads

$$I_{CL}^{\pm} = \frac{1}{\theta^{\pm}} \int_1^l \frac{(\widetilde{h}+H^{\pm})(\widetilde{h}-1)\, d\widetilde{h}}{k(\widetilde{h})\sqrt{\dfrac{\widetilde{\chi}}{C^{\pm}}\dfrac{1}{(\widetilde{h}+H^{\pm})^2} - \dfrac{1}{C^{\pm}}\dfrac{1}{\widetilde{h}^2} + 1}}, \qquad (18)$$

where $C^{\pm} = 1 - \widetilde{\chi}/(1+H^{\pm})^2$. It follows that

$$I_{CL}^{\pm} = \frac{1}{\theta^{\pm}} \int_1^{\infty} \left[\frac{(\widetilde{h}+H^{\pm})(\widetilde{h}-1)}{k(\widetilde{h})\sqrt{\dfrac{\widetilde{\chi}}{C^{\pm}}\dfrac{1}{(\widetilde{h}+H^{\pm})^2} - \dfrac{1}{C^{\pm}}\dfrac{1}{\widetilde{h}^2} + 1}} - \frac{3}{\widetilde{h}}\right] \times d\widetilde{h} + \frac{3}{\theta^{\pm}} \int_1^l \frac{1}{\widetilde{h}} d\widetilde{h} \equiv \frac{3}{\theta^{\pm}} \ln \delta^{\pm} l, \qquad (19)$$

where $\delta^{\pm} = \delta^{\pm}(H^{\pm}, \widetilde{\chi}, \lambda)$. In general $\delta^{\pm}$ must be computed numerically.

4.2.2 Bulk region

In the droplet bulk (BLK) region we may take the droplet to be thick, $(1, H^{\pm}) \ll lh_0$, and hence broad, $(1, H^{\pm}) \ll a$.

We write $h = \widetilde{h} + H^-$ and use a cap-like approximation for the drop shape, viz.,

$$\widetilde{h}\,(x) = \frac{1}{2}\theta^{\pm} a \left[1 - \left(\frac{x}{a}\right)^2\right] \tag{20}$$

near either contact line, where $\widetilde{h} \sim \mathcal{O}(l)$. With $\lambda \sim \mathcal{O}(1)$ the quantity (14) becomes

$$I^+_{BLK} = 3 \int_0^{a-l(\Delta H+1)} \frac{dx}{\widetilde{h}\,(x)} = \frac{3}{\theta^+} \ln \frac{2a}{l(\Delta H+1)}, \tag{21}$$

$$I^-_{BLK} = 3 \int_0^{a-l} \frac{dx}{\widetilde{h}\,(x)} = \frac{3}{\theta^-} \ln \frac{2a}{l}. \tag{22}$$

For a thick terrace, or equivalently for a system with $\tilde{\chi}/(H^{\pm})^2 \ll 1$, the corresponding results are obtained by replacing $C^{\pm}$ and $\theta^{\pm}$ by 1 and θ_0, respectively, where

$$\theta_0 \equiv \sqrt{\frac{3\beta n_0^2 |\chi|}{8\pi}}. \tag{23}$$

4.2.3 Droplet domain

The sum of the *bulk* and the *contact line* contributions finally reads

$$I = I^{\pm}_{CL} + I^{\pm}_{BLK} = \frac{3}{\theta_0}\left(\frac{\ln 2a\delta^+/(\Delta H+1)}{\sqrt{C^+}} + \frac{\ln 2a\delta^-}{\sqrt{C^-}}\right), \tag{24}$$

or, in the case of a thick terrace,

$$\widetilde{I} = \widetilde{I}^{\pm}_{CL} + \widetilde{I}^{\pm}_{BLK} = \frac{3}{\theta_0} \ln \frac{4a^2\widetilde{\delta}^+\widetilde{\delta}^-}{\Delta H+1}. \tag{25}$$

The final result is independent of l, as it must.

4.3 Droplet velocity

Equations (13) and (24) now yield an expression for the droplet velocity:

$$v = \frac{F^- - F^+}{I} = \frac{\theta_0^3}{6} \frac{\sqrt{C^+C^-}\,(C^+ - C^-)}{\sqrt{C^-}\ln\dfrac{2a\delta^+}{\Delta H+1} + \sqrt{C^+}\ln 2a\delta^-} \tag{26}$$

or, in the case of the thick terrace,

$$v \simeq \frac{F^- - F^+}{\widetilde{I}} = \frac{\theta_0^3}{6} \frac{C^+ - C^-}{\ln\left[4a^2\widetilde{\delta}^+\widetilde{\delta}^-/(\Delta H+1)\right]}. \tag{27}$$

Figure 7 compares the straightforward (26) and approximate (27) results with a direct numerical integration of equation (3). In all cases the droplet remains stationary whenever $\chi_\alpha = 0$ since $C^+ - C^-$ then vanishes, a result that is consistent with the asymptotic equilibrium condition (9). When this is not the case the droplet either ascends or descends the terrace according to the sign of χ_α until it reaches an equilibrium position. Sustained droplet motion is therefore possible only if the terrace is allowed to move as well, for example, due to melting or solidification of the liquid in contact with the solid [26].

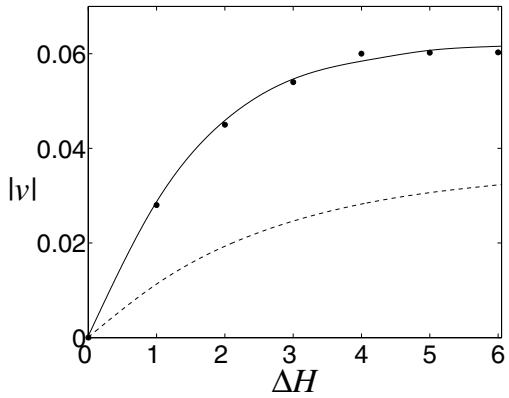

Fig. 7. Dependence of the velocity v on the terrace height ΔH. The solid/dashed lines represent the predictions (26) and (27) while the points represent numerical results obtained from equation (3). Parameters: $\beta = 15$, $\chi = -0.3$, $\mu_0 = -11.3636$, $n_0 = 0.9282$, $\chi_\alpha = -150$, $\lambda = \sqrt{3}$, $a \simeq 25$ and $H^- = 6$.

5 Conclusion

In this paper we have discussed several phenomena associated with the formation and motion of fluid droplets on composite substrates. The latter include substrates covered by a frozen phase of the liquid and dominated by van der Waals interactions. Our analysis centered on (a) the criteria for the formation of droplets on a uniform solid support, and (b) the translation of droplets on an *immobilized* terraced landscape. In the nonwetting case, we were able to obtain analytical conditions for droplet formation vs. instability (Eq. (8)). Instability is associated with the competition between van der Waals interactions through the molecular interactions (the effective Hamaker constant) and the composition height above the substrate, as shown in Figure 3. We also considered a large isothermal droplet on a terraced substrate for which both the precursor and the steps in the thickness of the solid phase are small compared to the droplet radius ($h_0^{\pm} \ll a$ and $\Delta H \ll a$, respectively). In this limit, we obtained analytical estimates for the droplet velocity (Eq. (26)) for comparison with the case in which contact angle asymmetry is due to horizontal thermal gradients [23] instead of differences in the disjoining potential. The results agree well with numerical solutions of the lubrication equation (3).

It should be emphasized that simultaneous droplet–terrace mobility due to support melting [23,26] does not correspond to a steady solution of the thin film equation [51] in the frame receding with the terrace edge. As the terrace melts it augments continuously, albeit slowly,

the volume of the liquid in the system. Consequently the volume of the droplet attached to the terrace edge must increase monotonically. It is reasonable to anticipate that once the droplet becomes too distended the instability of Section 3.2 kicks in and leads to the shedding of smaller droplets.

The results obtained here should prove useful in additional experimental studies of the competition between material phase transitions and van der Waals interactions in both longitudinal and transverse directions. The latter is particularly significant in more complicated cases of droplet-droplet and droplet-terrace interactions, as reported in [26].

We are grateful to Hans Riegler and Uwe Thiele for helpful discussions. This research was supported by NASA (grant No. NNCO4GA47G) and by Israel Science Foundation (grant No. 55/02). One of us (A.Y.) thanks Vered Rom-Kedar and the Department of Applied Mathematics and Computer Science, Weizmann Institute of Science, for hospitality during the completion of this work.

Appendix A: Disjoining potential

In this appendix we provide a self-contained derivation of the disjoining potential, correcting several misprints in reference [23]. We assume that all interactions are dominated by the van der Waals type potential

$$V(r) = \begin{cases} -\dfrac{A_j}{r^6} \text{ for } r > d \\ \infty \quad \text{for } r \le d, \end{cases} \tag{28}$$

where d is the nominal hard-core molecular diameter. All interactions are described by the same hard core interaction potential differing only in the interaction strength, A (fluid-fluid), $A_t \equiv \alpha_t A$ (fluid-terrace) and $A_s \equiv \alpha_s A$ (fluid-substrate).

A.1 Fluid-vapor interface

In the absence of a support, the equilibrium particle density distribution $n(z)$ is obtained by minimizing the grand ensemble thermodynamic potential $\Phi \equiv \mathcal{F} - \mu_0 \int_{-\infty}^{\infty} n(z)\,dz$ [5], where

$$\mathcal{F} \equiv \int_{-\infty}^{\infty} n(z) f(n) dz + \frac{1}{2} \int_{-\infty}^{\infty} n(z)\,dz \int_{-\infty}^{\infty} Q(\zeta)[n(z+\zeta) - n(z)]\,d\zeta, \tag{29}$$

$Q(\zeta) \equiv Q(|\zeta|)$, and μ_0 is the equilibrium chemical potential. The first term in (29) is the free energy of a homogeneous fluid [10], with

$$f(n,T) = k_B T \ln \frac{bn}{1-bn} - an, \tag{30}$$

where T is the temperature, k_B is the Boltzmann constant, $b \equiv 2\pi d^3/3$ is the excluded volume and

$$a = -2\pi \int_d^{\infty} V(r) r^2\,dr = \frac{2\pi A}{3d^3}; \tag{31}$$

in the following we are interested in the regime where the function $F(n) \equiv n[f(n) - \mu_0]$ has two minima $n^{\pm}$, corresponding to two stable uniform equilibrium states of higher and lower density (liquid and vapor). The second term in (29) accounts for inhomogeneous molecular interactions within the lubrication assumption, i.e., between the layers $z =$ constant [10]:

$$Q(\zeta) = \begin{cases} -\dfrac{\pi}{2\zeta^4} A \text{ for } |\zeta| > d, \\ -\dfrac{\pi}{2d^4} A \text{ for } |\zeta| \le d. \end{cases} \tag{32}$$

The condition for the minimum of the grand ensemble thermodynamic potential is

$$\frac{d[nf(n)]}{dn} + \int_{-\infty}^{\infty} Q(\zeta)[n(z+\zeta) - n(z)]\,d\zeta - \mu_0 = 0, \tag{33}$$

or, in dimensionless form,

$$\frac{1}{1-\widehat{n}} - \ln\left(\frac{1}{\widehat{n}} - 1\right) - 2\beta\widehat{n} - \widehat{\mu}_0 + \frac{3}{4}\beta \int_{-\infty}^{\infty} Q(\zeta)[\widehat{n}(z+\zeta) - \widehat{n}(z)]\,d\zeta = 0. \tag{34}$$

Here $Q(\zeta) = -\zeta^{-4}$, $|\zeta| > 1$; $Q(\zeta) = -1$, $|\zeta| \le 1$, and $\beta = A/(k_B T d^6)$ is the dimensionless inverse temperature. To obtain this expression we have scaled lengths by d, the particle density by $1/b$ and the chemical potential by $k_B T$.

The interface width between the vapor and liquid as well as their densities depend on the inverse dimensionless temperature β. As shown in Figure A1, for higher β the interface width is of order of unity or in real units of order of the molecular scale d, and the vapor density at this value is negligible. The experiments on the long chain alkane system [25] were conducted in this regime. Consequently in all computations we used values for the equilibrium chemical potential $\widehat{\mu}_0$ and fluid density $\widehat{n}^+$ obtained from the Maxwell construction [5] at $\beta = 15$.

A.2 Solid-fluid-vapor system

In the proximity of the support the equilibrium chemical potential is shifted from the Maxwell result $\mu = \mu_0$, and the fluid interface position h is defined to be at the Gibbs surface [11]. The liquid in the vicinity of the freezing point coexists with a solid phase, so that we assume that the support includes both the substrate and frozen phase, as

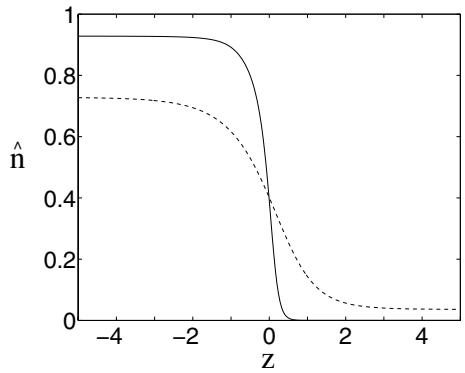

Fig. A1. The particle density profiles $\widehat{n}$ of the liquid-vapor interface at $\beta = 15$ (solid line) and $\beta = 5$ (dashed line) computed numerically from equation (34). The location $z = 0$ refers to the equivalent sharp interface location.

shown in Figure 1. The free energy of the resulting film is given by [23]

$$\mathcal{F} = \int_H^\infty n(z) \left\{ f(n,T) - \frac{1}{2}\int_{-\infty}^{H} Q(z-\zeta)n(z)d\zeta + \frac{1}{2}\int_H^\infty Q(z-\zeta)[n(\zeta)-n(z)]\,d\zeta + \alpha_t n_t \int_0^H Q(z-\zeta)d\zeta + \alpha_s n_s \int_{-\infty}^{0} Q(z-\zeta)d\zeta \right\} dz. \quad (35)$$

Here $n(z)$, n_t, n_s are the liquid, terrace and substrate particle densities, and H is the thickness of the solid layer on top of the substrate. The second term in (35) compensates lost inhomogeneous fluid-fluid interactions in the domain $z < H$; the third term accounts for the inhomogeneous part of the fluid-fluid interactions above the support $z > H$; the last two terms account for the fluid-terrace and fluid-substrate interactions.

The corresponding Euler-Lagrange equation for the equilibrium density profile $n(z)$ is obtained by minimizing $\Phi = \mathcal{F} - \mu\int_H^\infty n(z)\,dz$ and reads

$$\frac{d[nf(n)]}{dn} + \int_H^\infty Q(z-\zeta)[n(\zeta)-n(z)]\,d\zeta - \mu - n(z)\int_{-\infty}^{H} Q(z-\zeta)d\zeta + \alpha_t n_t \int_0^H Q(z-\zeta)d\zeta + \alpha_s n_s \int_{-\infty}^{0} Q(z-\zeta)d\zeta = 0, \quad (36)$$

where $\mathcal{F}$ is given by equation (35). The first three terms in equation (36) are analogous to the three terms in equation (33) but are computed over the fluid-vapor domain only; the remaining three terms arise from energy distortion due to the solid support.

A.2.1 Droplet bulk

We identify the effective disjoining potential with the shift in the chemical potential per unit volume relative to the equilibrium value μ_0, $\Pi(n) \equiv n[\mu(n) - \mu_0]$ [7]. In the *bulk* region, $H + d < z < h$, we may take the fluid density to be constant, $n \simeq n^+ \equiv n_0$, and neglect the density in the vapor phase in $z > h$: $n^- = 0$ [52]. Thus $\Pi \equiv \Pi(h)$, and using equations (33) and (36) it is now a simple matter to obtain the (dimensional) disjoining potential in the bulk:

$$\Pi(h) = -\frac{\pi A n_0^2}{6}\left[\frac{\chi}{(h-H)^3} + \frac{\chi_\alpha}{h^3}\right]. \quad (37)$$

Here $\chi \equiv \alpha_t n_t/n_0 - 1$, $\chi_\alpha \equiv (\alpha_s n_s - \alpha_t n_t)/n_0$ are, respectively, the dimensionless Hamaker constants for the fluid-terrace and terrace-substrate interfaces. In the following we take $n_t = n_0$ since both the terrace and liquid are composed of the same material.

A.2.2 Fluid precursor

The experimental observations indicate that, under appropriate conditions, a thick film can coexist with a constant fluid precursor monolayer of molecular thickness [25]. Since the diffuse interface varies significantly on molecular scales the computation of the chemical potential in the precursor region must allow for density changes.

An analogous calculation of the disjoining potential $\Pi(n) \equiv n[\mu(n) - \mu_0]$ evaluated at $z = H + d$ now leads to the result

$$\Pi(n) = -\frac{\pi A n}{6}\left[\frac{n_0(\chi+1)-n}{d^3} + \frac{\chi_\alpha n_0}{(H+d)^3}\right] + n\left[\frac{d(nf)}{dn} - \mu_0\right]. \quad (38)$$

Since $d[n_0 f(n_0)]/dn_0 = \mu_0$ at $h = H + d$, the disjoining potential is continuous across the entire fluid domain.

Appendix B: Numerical computation

Numerical integration of equation (3) was performed using an explicit spectral method [53]. In cases where the terrace topography was included we doubled the domain size to effectively impose reflecting boundary conditions (not shown in the figure). Moreover, since the terrace involves a discontinuity we have replaced the sharp transition ΔH (solid line within the support domain in Fig. 6b) by a smooth function $\propto \tanh(x/\sqrt{\Delta H})$ (shaded region in Fig. 6b). This phenomenological treatment is also required by the physical scaling leading to the lubrication model. We emphasize that as long as the terrace lies within the

droplet domain and the droplet radius is large compared with the terrace height, the smoothing of the terrace profile has only a minor effect on the results since the disjoining potential falls off as $\Pi \sim h^{-3}$.

References

1. J. Eggers, Rev. Mod. Phys. **69**, 865 (1997)
2. U. Thiele, Eur. Phys. J. E **12**, 409 (2003)
3. P.G. de Gennes, Rev. Mod. Phys. **57**, 827 (1985)
4. A. Oron, S.H. Davis, S.G. Bankoff, Rev. Mod. Phys. **69**, 931 (1997)
5. L.M. Pismen, Colloids Surfaces A-Physicochem. Eng. Aspects **206**, 11 (2002)
6. L.M. Pismen, Y. Pomeau, Phys. Fluids **16**, 2604 (2004)
7. B.V. Derjaguin, N.V. Churaev, V.M. Muller, *Surface Forces* (Consultants Bureau, New York, 1987)
8. A. Sharma, Langmuir **9**, 861 (1993)
9. A. Sharma, Langmuir **9**, 3580 (1993)
10. L.M. Pismen, Phys. Rev. E **64**, 21603 (2001)
11. L.M. Pismen, Y. Pomeau, Phys. Rev. E **62**, 2480 (2000)
12. F. Brochard, Langmuir **5**, 432 (1989)
13. M.G. Velarde, Philos. Trans. R. Soc. London A **356**, 859 (1998)
14. E. Raphaël, C. R. Acad. Sci. Ser. II **306**, 751 (1988)
15. M.K. Chaudhury, G.M. Whitesides, Science **256**, 1539 (1992)
16. A.Y. Rednikov, Y.S. Ryazantsev, M.G. Velarde, Phys. Fluids **6**, 451 (1994)
17. C.D. Bain, G.D. Burnetthall, R.R. Montgomerie, Nature (London) **372**, 414 (1994)
18. F. Domingues Dos Santos, T. Ondarçuhu, Phys. Rev. Lett. **75**, 2972 (1995)
19. A.S. Mikhailov, D. Meinköhn, in Lecture Notes in Physics, edited by L. Schimansky-Geier, T. Pöschel (Springer, Berlin, 1997), Vol. 484, p. 334
20. S.W. Lee, D.Y. Kwok, P.E. Laibinis, Phys. Rev. E **65**, 51602 (2002)
21. U. Thiele, K. John, M. Bär, Phys. Rev. Lett. **93**, 27802 (2004)
22. Y. Sumino, N. Magome, T. Hamada, K. Yoshikawa, Phys. Rev. Lett. **94**, 68301 (2005)
23. A. Yochelis, L.M. Pismen, Phys. Rev. E **72**, R25301 (2005)
24. L.M. Pismen, Phys. Rev. E **74**, 41605 (2006)
25. P. Lazar, H. Schollmeyer, H. Riegler, Phys. Rev. Lett. **94**, 116101 (2005)
26. P. Lazar, H. Riegler, Phys. Rev. Lett. **95**, 136103 (2005)
27. C. Ebner, W.F. Saam, Phys. Rev. Lett. **38**, 1486 (1977)
28. H. Nakanishi, M.E. Fisher, Phys. Rev. Lett. **49**, 1565 (1982)
29. R. Lipowsky, D.M. Kroll, Phys. Rev. Lett. **52**, 2303 (1984)
30. S. Dietrich, M. Schick, Phys. Rev. B **31**, 4718 (1985)
31. D. Ross, D. Bonn, J. Meunier, Nature (London) **400**, 737 (1999)
32. D. Bonn, E. Bertrand, N. Shahidzadeh, K. Ragil, H.T. Dobbs, A.I. Posazhennikova, D. Broseta, J. Meunier, J.O. Indekeu, J. Phys.: Condens. Mat. **13**, 4903 (2001)
33. A. Yochelis, L.M. Pismen, Colloids Surfaces A-Physicochem. Eng. Aspects **274**, 170 (2006)
34. T. Pfohl, H. Riegler, Phys. Rev. Lett. **82**, 783 (1999)
35. E. Ruckenstein, R. Jain, J. Chem. Soc., Faraday Trans. 2 **70**, 132 (1974)
36. H.S. Kheshgi, L.E. Scriven, Chem. Eng. Sci. **46**, 519 (1991)
37. G. Reiter, Phys. Rev. Lett. **68**, 75 (1992)
38. V.S. Mitlin, J. Colloid Interface Sci. **156**, 491 (1993)
39. J. Bischof, D. Scherer, S. Herminghaus, P. Leiderer, Phys. Rev. Lett. **77**, 1536 (1996)
40. R. Xie, A. Karim, J. Douglas, C. Han, R. Weiss, Phys. Rev. Lett. **81**, 1251 (1998)
41. U. Thiele, M. Mertig, W. Pompe, Phys. Rev. Lett. **80**, 2869 (1998)
42. K. Jacobs, S. Herminghaus, K.R. Mecke, Langmuir **14**, 965 (1998)
43. G. Reiter, A. Sharma, A. Casoli, M.-O. David, R. Khanna, P. Auroy, Langmuir **15**, 2551 (1999)
44. R. Khanna, A. Sharma, G. Reiter, EPJdirect E **2**, 1 (2000)
45. U. Thiele, M. G. Velarde, K. Neuffer, Y. Pomeau, Phys. Rev. E **64**, 31602 (2001)
46. L.M. Pismen, U. Thiele, Phys. Fluids **18**, 42104 (2006)
47. K.B. Glasner, T.P. Witelski, Phys. Rev. E **67**, 16302 (2003)
48. L.M. Pismen, Phys. Rev. E **70**, 21601 (2004)
49. M.N. Popescu, S. Dietrich, Phys. Rev. E **93**, 61602 (2004)
50. M. Oron, T. Kerle, R. Yerushalmi-Rozen, J. Klein, Phys. Rev. Lett. **92**, 236104 (2004)
51. U. Thiele, E. Knobloch, Phys. Rev. Lett. **97**, 204501 (2006)
52. S. Dietrich, M. Napiórkowski, Phys. Rev. A **43**, 1861 (1991)
53. J. Zhu, L.-Q. Chen, J. Shen, V. Tikare, Phys. Rev. E **60**, 3564 (1999)